

# Fast Fourier backprojection for frequency-domain optoacoustic tomography

Pouyan Mohajerani, Stephan Kellnberger, and Vasilis Ntziachristos\*

*Institute for Biological and Medical Imaging, Technical University of Munich and Helmholtz Zentrum München, Ingolstädter Landstrasse 1, Neuherberg 85764, Germany*

\*Corresponding author: v.ntziachristos@tum.de

Received July 11, 2014; accepted August 6, 2014;

posted August 13, 2014 (Doc. ID 216877); published September 15, 2014

We present a time-efficient backprojection image reconstruction approach applied to frequency-domain (FD) optoacoustic tomography based on tissue illumination at multiple, discrete frequencies. The presented method estimates the Fourier transform of a spatial, circular profile of the underlying image using the amplitude and phase data. These data are collected over multiple frequencies using an acoustic transducer positioned at several locations around the sample. Fourier-transform values for absent frequencies are estimated using interpolation based on low-pass filtering in the image domain. Reconstruction results are presented for synthetic measurements using numerical phantoms, and the results are compared with FD model-based reconstructions. © 2014 Optical Society of America

OCIS codes: (170.3880) Medical and biological imaging; (170.5120) Photoacoustic imaging; (170.6960) Tomography.  
<http://dx.doi.org/10.1364/OL.39.005455>

Optoacoustic tomography is typically implemented using nanosecond pulses due to the favorable signal-to-noise characteristics offered when powerful lasers are employed. However, optoacoustic signal generation occurs with any transient light intensity absorbed by tissue. Correspondingly, sinusoidal optical intensity modulated in frequency using chirp has been employed for optoacoustic imaging using raster scan of a light beam [1] or multi-projection tomography [2]. Chirp modulation encodes time onto frequency: time delays are encoded on different frequency values. Detection is then based on cross correlation of the detected signal with a reference signal coming from the modulated source. A characteristic of chirp-based optoacoustic detection is that the frequency emitted onto the target at any given time is not contained in the frequency band detected at that same time.

We have recently presented frequency-domain (FD) optoacoustic tomography which utilizes sinusoidal optical intensity and detects complex acoustic measurements obtained through continuous excitation of the target [3]. In contrast to chirp-based imaging, FD optoacoustic tomography has no dependence on time or time delay. Therefore, while it preferably utilizes multiple, distinct frequencies, these frequencies can be emitted and detected simultaneously. Independently from the number of frequencies employed (one or multiple), FD optoacoustics based on illumination with light always detect exactly the frequency or frequencies emitted at the target.

The principle of optoacoustic imaging using FD measurements was showcased using model-based image reconstruction based on least-squares minimization and Tikhonov regularization [3]. In this approach, a linear model of the system is constructed, where a weight matrix relates the acoustic measurements to the heat source distribution (or the optical absorption). The weight matrix elements are derived from the FD wave equation. The model-based method presented in [3] is a flexible approach capable of accurately reconstructing in arbitrary geometries. This method also lends itself to incorporation of the detector models [4]. While model-based inversion yields high imaging accuracy, it is generally time-consuming due to the large volume of numerical

computations required. Typically several tens of seconds are needed for a 2D image with 10,000 reconstruction voxels. Such metrics make this method inappropriate for real-time imaging implementations.

Instead, we propose herein a backprojection-based algorithm for inversion of FD data, i.e., amplitude and phase measurements of propagating acoustic waves collected over multiple, distinct frequencies and projections. The proposed method uses fast Fourier transform (FFT) to achieve real-time reconstruction for tissue dimensions as large as 2 cm and several tens of frequencies used. Backprojection methods are common in time-domain optoacoustic tomography, i.e., when using short-pulse illumination [5,6]. These methods are often based on analytical formulas, derived in time or frequency domains using diffraction tomography concepts [5,7,8]. Nevertheless, such backprojection methods have been demonstrated often in the context of time-domain optoacoustic tomography, and are often limited to the specific configuration of detectors. The backprojection FFT (BPFFT) method proposed herein is particularly developed for FD optoacoustic tomography using multiple, distinct frequencies.

The proposed method is further applicable to arbitrary geometries and detector configurations. For simplicity and without loss of generality, we consider the circular geometry depicted in Fig. 1, where the detectors are placed around the sample at  $D$  locations  $\theta_i, i = 1 \dots D$ . The sound speed is assumed to have a constant value of  $c_a$  within the sample. Let  $x(v)$  denote the unknown absorbed energy density at voxel  $v$ . Then

$$x(v) = \mu_a(v)I_a(v), \quad (1)$$

where  $\mu_a(v)$  and  $I_a(v)$  denote the optical absorption coefficient and the fluence at voxel  $v$ , respectively. In this Letter we reconstruct the property  $x(v)$ . Methods developed to separate the optical absorption from fluence terms can then be employed [9].

The acoustic signal measured at angle  $\theta$  at the angular frequency  $\omega = 2\pi f$  can then be written as

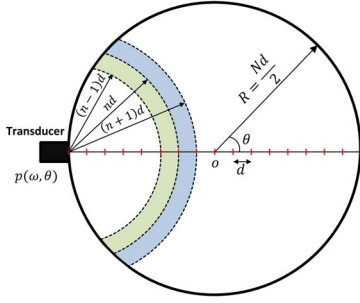


Fig. 1. Concept of the proposed BPFFFT algorithm; for a given projection angle  $\theta$  (here  $\theta = \pi$ ) the reconstruction area is divided to circular slices, where the  $n$ th circle has a radius of  $nd$ . The diameter is divided into  $N$  subdivisions (red marks) of length  $d$ . The green or blue slices denote circular slices  $A_n(\theta)$ , and are geometrical loci of voxels with the same contribution to  $p(\omega, \theta)$ .

$$p(\omega, \theta) = -i\omega\gamma \sum_v \frac{e^{ikr_v(\theta)}}{r_v(\theta)} x(v), \quad (2)$$

where  $k$  is the wave number given as  $k = \omega/c_a$ .  $r_v(\theta)$  denotes the distance of the voxel  $v$  from the transducer at projection angle  $\theta$  [3]. The constant  $\gamma$  is given as

$$\gamma = \frac{-\beta v}{4\pi C_p} e^{i\phi_a}, \quad (3)$$

where  $\beta$  is the thermal expansion coefficient,  $C_p$  is the specific heat capacity,  $v$  is the dimensionless energy conversion efficient, and  $\phi_a$  is a phase constant due to the thermo-elastic conversion of tissue [3].  $\gamma$  is a multiplicative factor which is omitted from the formulations for simplicity.

The diagonal line passing through the transducer location (the diagonal shown in Fig. 1) is partitioned into  $N$  segments of length  $d$ . Let  $A_n(\theta)$  denote a circular slice of the sample obtained over the  $n$ th segment for detection angle  $\theta$ , as shown in Fig. 1. Define  $y(n)$  as the summation of the vector  $x$  within each slice

$$y(n) = \sum_{v \in A_n(\theta)} x(v). \quad (4)$$

Subsequently, the measured pressure wave  $p(\omega, \theta)$  is normalized by the respective  $\omega$  as

$$\bar{p}(\omega, \theta) = \frac{p(\omega, \theta)^*}{i\omega}, \quad (5)$$

where  $*$  denotes complex conjugate. Then  $\bar{p}(\omega, \theta)$  can be estimated as

$$\bar{p}(\omega, \theta) = \sum_v \frac{e^{-ikr_v(\theta)}}{r_v(\theta)} x(v) \approx \sum_{n=1}^N e^{-iknd} \frac{y(n)}{nd - \frac{d}{2}}, \quad (6)$$

where  $r_v(\theta)$  is approximated by the detector distance from the midpoint of the  $n$ th circular arc, i.e.,  $nd - d/2$ . Next, we assume  $M$  discrete frequencies emitted to the target. We assume an equispaced frequency

distribution where the  $m$ th frequency  $\omega_m = 2\pi f_m$  can be expressed as

$$f_m = f_0 + (m-1)\Delta f, \quad m = 1 \dots M, \quad (7)$$

where  $\Delta f$  is the frequency step. The method is, nonetheless, readily generalizable to nonuniform frequency distributions. By defining  $z(n) = y(n)/nd - d/2$  and combining Eqs. (4)–(7), we can write

$$\bar{p}(\omega, \theta) \approx \sum_{n=1}^N e^{-2\pi i((m-1)\Delta f + f_0)n \frac{d}{c_a}} z(n) e^{-2\pi i(m-1)(n-1) \frac{d\Delta f}{c_a}}. \quad (8)$$

A variable  $s_m(\theta)$  can be define using the normalized measurement  $\bar{p}$  as

$$s_m(\theta) = \bar{p}(2\pi f_m, \theta) e^{2\pi i(m-1) \frac{d\Delta f}{c_a}}. \quad (9)$$

Also, the complex sequence  $h(n)$  is defined as

$$h(n) = e^{-2\pi i \frac{f_0}{c_a} nd} z(n). \quad (10)$$

Then by combining Eqs. (8)–(10) we have

$$s_m(\theta) \approx \sum_{n=1}^N h(n) \left( e^{-2\pi i(m-1)(n-1) \times \frac{2R\Delta f}{Nc_a}} \right), \quad (11)$$

where  $R$  is the radius of the detector ring (Fig. 1). The parameter  $\alpha = 2R\Delta f/c_a$  is in the general case a real positive number. We approximate  $\alpha$  by a rational number. Specifically, let  $q_1$  and  $q_2$  be mutually prime integers such that  $q_2$  is a power of 2 and

$$\alpha \approx \frac{q_1}{q_2}. \quad (12)$$

In this Letter,  $q_2 = 32$  was chosen and observed to result in satisfactory approximation of  $\alpha$ . Also we define  $\bar{h}(n)$  as a  $1 \times Nq_2$  vector denoting the zero-padded version of  $h(n)$ , i.e.,

$$\bar{h} = [h0_{N(q_2-1)}]. \quad (13)$$

Hence, Eq. (11) can be written as

$$s_m(\theta) \approx \sum_{n=1}^{Nq_2} \bar{h}(n) \left( e^{-2\pi i \times \frac{(q_1(m-1)+1)(n-1)}{Nq_2}} \right). \quad (14)$$

The right side of this equation is recognized as the  $Nq_2$ -point discrete Fourier transform of the complex sequence  $\bar{h}(n)$ . Therefore we can write

$$s_m(\theta) \approx \mathcal{F}_{Nq_2}(\bar{h}(n), q_1(m-1) + 1), \quad (15)$$

where  $\mathcal{F}_P(a(n), m)$  denotes the  $m$ th discrete  $P$ -point Fourier-transform value of the sequence  $a(n)$ .

Inversion is then performed via backprojection. Specifically, for every angle  $\theta$  the measured signal at frequencies  $f_m$  forms  $M$  samples of the  $Nq_2$ -point FT of  $h(n)$ . The number  $N$  is chosen to be a power of 2 to enable application of the FFT. In this Letter,  $N$  was chosen as

$$N = 2^d, \quad d = \log_2(M \max(1, \alpha)) + 2, \quad (16)$$

where  $x$  denotes the ceil of  $x$ . The sequence  $s_m(\theta)$  is a down-sampled version (by a factor of  $q_1$ ) of the  $Nq_2$ -point FFT of  $\tilde{h}(n)$ . Instead of up-sampling  $s_m(\theta)$  and then performing inverse FFT (IFFT), we can low-pass filter the IFFT of  $s_m(\theta)$  by keeping only the first  $N$  samples. Low-pass filtering in the IFFT domain has the same impact as interpolation in the FFT domain. However, if the used frequencies  $f_m$  are nonuniformly distributed, then the sequence  $s_m(\theta)$  should be interpolated at the locations of missing frequencies prior to IFFT.

After we perform IFFT for every angle, the first  $N$  samples of the resulting signal form an approximation of  $h(n)$ , denoted by  $\tilde{h}(n)$ . Using Eq. (10), an estimation of  $y(n)$ , called  $\tilde{y}(n)$ , can be obtained from  $\tilde{h}(n)$ . The absolute value of sequence  $\tilde{y}(n)$  is then mapped to the 2D domain image update,  $x_\theta(v)$ . This mapping is given as

$$x_\theta(v) = \text{Re}[\tilde{y}(n)] \times \left( nd - \frac{d}{2} \right) \quad \text{where } v \in A_n(\theta), \quad (17)$$

where Re is the real part. The operation in Eq. (17) can be recognized as the backprojection of the 1D sequence on the right-hand side over the 2D domain.

The absorption image is then updated (starting from an all-zero image) by the 2D projection for each angle, i.e.,  $x_\theta(v)$ , as

$$x(v) \approx \sum_{i=1, \dots, D} x_{\theta_i}(v). \quad (18)$$

The reconstructed image  $x$  contains blurring artifacts, typical in backprojection algorithms. Hence, the image  $x$  is filtered in the  $k$ -space by a 2D Ram-Lak filter, defined as  $f(k_1, k_2) = \sqrt{k_1^2 + k_2^2}$ , where  $k_1$  and  $k_2$  are  $k$ -space coordinates. A summary of the proposed method is also presented in Table 1.

**Table 1 Proposed BPFIT Algorithm**

- i. Initialization:  $x = 0_v, j = 1$ .
- ii. Set  $\theta = \theta_j$  and define  $e = 0_{Nq_2}$ .
- iii. Define  $\tilde{p}(\omega, \theta) = \frac{p(\omega, \theta)}{i\omega}$ .
- iv. Mapping<sup>a</sup>:  $m = 1 \dots M$ ,

$$e(q_1(m-1) + 1) = \tilde{p}(2\pi f_m, \theta)$$

- v. Inverse FFT:  $g = \mathcal{F}_{Nq_2}^{-1}(e)$ .
- vi. Cropping:  $h^c = g(1, \dots, N)$ .
- vii. Unweighing: for all voxels  $v$

- a. Find  $n$ ; such that  $v \in A_n(\theta)$ .

$$b. \quad x_\theta(v) = \text{Re} \left[ h^c(n) e^{+ \frac{2\pi i f_0 n d}{c_a}} \right] \times \left( nd = \frac{d}{2} \right).$$

- viii. Update:  $\forall v, x(v) = x(v) + x_\theta(v)$ .
- ix. If  $j \leq D$  go to step ii.
- x. Applying a Ram-Lak filter to  $x$  in the  $k$ -space.
- xi. Termination:  $x \rightarrow$  solution

<sup>a</sup>Values of  $q_1$  and  $q_2$  are defined in Eq. (12).

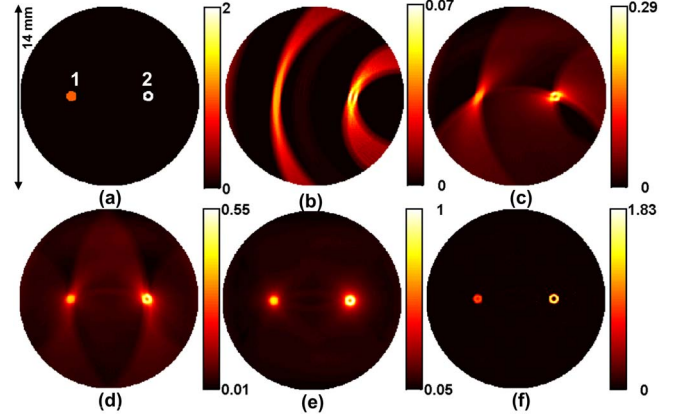


Fig. 2. Evolution of BPFIT across projection; (a) true image of a numerical phantom with a diameter of 14 mm and two absorbing objects numbered 1 and 2 (respectively, filled and hollow) with absorptions of  $\mu_0$  and  $2\mu_0$ , respectively, and a diameter of 0.8 mm. Panels (b)–(e) show reconstructed absorption images for 10°, 45°, 90°, and 180° angles. (f) Final reconstructed image, after applying the 2-D Ram-Lak filter to (e). 45 frequencies between 300 KHz and 4.7 MHz in steps of 100 KHz were used. Detection was performed on 180 locations, and the reconstruction resolution was 70  $\mu\text{m}$ . The parameter  $\mu_0$  is not shown on the depicted scales for simplicity.

The BPFIT method is verified using simulation results for a circular phantom with a diameter of 14 mm, containing two absorbing objects, as shown in Fig. 2(a). The objects 1 and 2 had optical absorptions of  $\mu_0$  and  $2\mu_0$ , respectively. Objects 1 and 2 were a filled circle and a ring shape, respectively. Objects were designed as such to evaluate BPFIT's performance in preserving content. The parameter  $\mu_0$  was set to a typical tissue optical absorption value of 0.3  $\text{cm}^{-1}$ . For simplicity the parameter  $\mu_0$  is not shown in the graphs. For the sample diameter of 14 mm, the parameter  $q_1$  in Eq. (12) was found to be 30. Simulations were performed for 180 equispaced detectors positioned around the sample and 45 illumination frequencies between 300 KHz to 4.8 MHz in steps of 100 KHz. Figures 2(b)–2(e) demonstrate the evolution of the image reconstructed using BPFIT for a different number of detectors, when no noise is added to the measurements. Figure 2(f) shows the final reconstruction, after application of the Ram-Lak filter. The effect of noise was additionally simulated by adding white Gaussian noise to the synthetic measurement. Figure 3 shows the reconstruction of a T-shaped object, [Fig. 3(a)] for

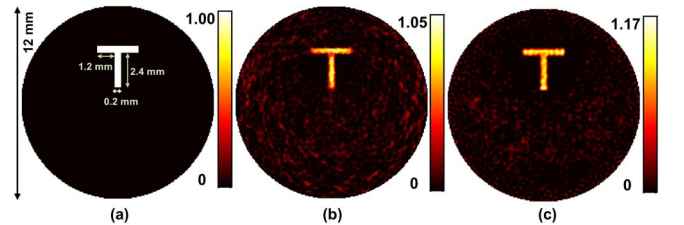


Fig. 3. Reconstruction of a T-shape object in presence of noise for an SNR of  $-5$  dB; (a) true image, (b) BBPFIT reconstruction, (c) LSQR reconstruction with 100 iterations. 45 frequencies between 300 KHz and 4.8 MHz, in steps of 100 KHz were used. Detection was performed on 180 locations, and the reconstruction resolution was 70  $\mu\text{m}$ .

noisy measurements with a signal-to-noise ratio (SNR) of  $\sim -5$  dB (i.e., noise power around 4.5 times stronger than the signal power). The additive noise was simulated using zero-mean Gaussian random variables for both the real and imaginary parts, as explained in [3]. For this case, 45 frequencies from 0.3 to 5 MHz and 300 detector locations were used. The phantom had a diameter of 12 mm ( $q_1 = 26$ ,  $q_2 = 32$ ), and the reconstruction resolution was 70  $\mu\text{m}$ . Figures 3(b) and 3(c) show reconstructions using BPFFFT and using a model-based approach, respectively. The model-based approach used the least-square method (LSQR) [10] with 100 iterations [3]. The entire BPFFFT reconstruction lasted 0.10 s on a computer with an Intel Core i7 CPU @ 3.4 GHz and 16 GB RAM. The model-based reconstruction lasted 89.6 s.

Both circular objects can be differentiated in Fig. 2(f). Objects 1 and 2 are further reconstructed as a circle and a ring, respectively, both with diameters of  $\sim 8.3$  mm. The ratios of the intensities (averaged within respective object areas) of the reconstructed objects were 1.95, respectively, which is very close to the true ratios of 2. However, the absolute reconstructed values are almost half of the true values. This phenomenon is due to the limited bandwidth of the illumination frequencies. In Fig. 3, the T-shape is well recognizable using both BPFFFT and LSQR approaches, although the latter has a much higher accuracy. However, FPFFFT reconstruction was approximately 900 times faster than the model-based reconstruction. This feature of BPFFFT enables real-time imaging with frame rates as high as 10 frames/s, for the system settings of Fig. 3. Moreover, while the memory and computation time of BPFFFT grows linearly with the sample diameter, model-based reconstruction burden grows with the square of the sample diameter. The results were presented for a circular phantom with equispaced frequencies and detection angles. Nevertheless, the proposed approach can be readily implemented for

arbitrary geometries, detector configurations, and frequency distributions with full and limited view data in both two and three dimensions. The extension to 3D follows by defining spherical slices (instead of circular arcs). A 1D Fourier-transform relationship, similar to Eq. (15), then holds, with  $y(n)$  defined as the integration of the 3D solution over the slices.

In conclusion, we presented a fast backprojection method based on FFT for real-time reconstruction of absorption images in FD optoacoustic tomography. The proposed method uses amplitude and phase data over multiple, discrete frequencies to reconstruct the absorption image. Extensions for detector configurations and spatial and frequency samplings are possible. These generalizations as well as the trade-offs governing different systems, models, and parameters are subjects of ongoing research.

## References

1. S. Telenkov, A. Mandelis, B. Lashkari, and M. Forcht, *J. Appl. Phys.* **105**, 102029 (2009).
2. S. Kellnberger, N. C. Deliolanis, D. Queiros, G. Sergiadis, and V. Ntziachristos, *Opt. Lett.* **37**, 3423 (2012).
3. P. Mohajerani, S. Kellnberger, and V. Ntziachristos, *Photoacoustics* **3**, 111 (2014).
4. A. Rosenthal, D. Razansky, and V. Ntziachristos, *IEEE Trans. Med. Imaging* **29**, 1275 (2010).
5. M. Xu and L. V. Wang, *Phys. Rev. E* **71**, 016706 (2005).
6. R. A. Kruger, P. Liu, and C. R. Appledorn, *Med. Phys.* **22**, 1605 (1995).
7. S. J. Norton and T. Vo-Dinh, *J. Opt. Soc. Am. A* **20**, 1859 (2003).
8. N. Baddour, *J. Acoust. Soc. Am.* **123**, 2577 (2008).
9. A. Rosenthal, T. Jetzfellner, D. Razansky, and V. Ntziachristos, *IEEE Trans. Med. Imaging* **31**, 1346 (2012).
10. C. C. Paige and M. A. Saunders, *ACM Trans. Math. Softw.* **8**, 43 (1982).